actuators

MDPI

Review

Core–Shell Magnetoelectric Nanoparticles: Materials, Synthesis, Magnetoelectricity, and Applications

Hyunseok Song [1], Michael Abraham Listyawan [1] and Jungho Ryu [1,2,*]

[1] School of Materials Science and Engineering, Yeungnam University, Daehak-ro, Gyeongsan-si 38541, Gyeongsangbuk-do, Republic of Korea
[2] Institute of Materials Technology, Yeungnam University, Daehak-ro, Gyeongsan-si 38541, Gyeongsangbuk-do, Republic of Korea
* Correspondence: jhryu@ynu.ac.kr

Abstract: Nanoparticles with small diameters and large surface areas have potential advantages and are actively utilized in various fields related to biomedical and catalytic applications. Multifunctional applications can be achieved by endowing nanoparticles with piezoelectric, quantum dot, magnetothermal, and piezoluminescent properties. In particular, multiferroic magnetoelectric nanoparticles (MENPs) can generate electricity by coupling piezoelectric and magnetostrictive properties when an external magnetic field, which is harmless to the human body, is applied. In this regard, magnetoelectricity (ME) induced by a magnetic field makes MENPs useful for various biomedical and electrocatalytic applications. The ME voltage coefficients, which express the efficiency of energy conversion from magnetic field to electricity, show differences depending on the setup for ME measurements of MENPs. Therefore, numerous attempts have been made to optimize the ME characterization method to reduce measurement errors resulting from charge leakages caused by the specimen preparation, as well as to investigate the ME effect of a single nanoparticle. Our review is focused on the structures, syntheses (hydrothermal and sol–gel methods), activation mechanism, and measurement of magnetoelectricity, as well as applications, of core–shell MENPs.

Keywords: magnetoelectric effect; core–shell magnetoelectric nanoparticles; drug delivery; brain imaging; brain stimulation; cell regeneration; electrocatalyst

Citation: Song, H.; Listyawan, M.A.; Ryu, J. Core–Shell Magnetoelectric Nanoparticles: Materials, Synthesis, Magnetoelectricity, and Applications. *Actuators* **2022**, *11*, 380. https://doi.org/10.3390/act11120380

Academic Editor: Manfred Kohl

Received: 4 December 2022
Accepted: 15 December 2022
Published: 16 December 2022

1. Introduction

In recent years, nanoparticles have attracted great attention in various application fields [1–3], especially where movement in a microchannel and high reactivity are critical parameters, owing to their small size and large surface area. Because of these advantages, research trends are progressing in the direction of expanding the scope of applications by equipping nanoparticles with various multifunctions in biomedical and environmental applications [4–6]. For example, targeted tissues in the human body can be imaged or photostimulated using irradiation with near-infrared rays and quantum dot nanoparticles injected into the body [7–9]. Piezoelectric nanoparticles activated by mechanical vibrations, such as ultrasonic waves, generate electrical signals and transfer them to cells to promote cell proliferation and differentiation [10–12]. In addition, for hyperthermia therapy, the magnetothermal phenomenon, which occurs when a high-frequency alternating magnetic field is applied to magnetic nanoparticles, is employed [13]. As such, there is also a high need for multifunctional nanoparticles, as proven by recent studies.

The magnetoelectric (ME) phenomenon, which produces an electric field from an applied magnetic field or vice versa, is one of several multifunctions that have been applied to nanoparticles. It is primarily employed in research fields where it is advantageous to use a magnetic field as the driving source [14–25]. Based on these interactions, various applications related to the ME phenomenon, such as magnetic or current sensors [26,27],

memory devices [28], high energy density capacitors [29], energy harvesters [30], gyrators [31], resonators [32], inductors [33], ME antennas [34], and magneto-mechano-electric generators [35] have been developed. A high ME coupling effect is essential for the application of multiferroic magnetoelectric nanoparticles (MENPs) with high efficiency. The ME effect in multiphase ME composites is superior to that in single-phase ME materials [36]. Thus, in most applications, ME composite structured MENPs are generally synthesized as core–shell structured composites consisting of a magnetostrictive material, which converts a magnetic field into strain, and a piezoelectric material, which further converts stress from the magnetostrictive strain into an electric field. Generally, sol–gel [37] and hydrothermal methods [38,39] are intensively used to fabricate core–shell MENPs. As the synthesis methods are diverse, the methods for evaluating ME voltage coefficients are also diverse, including the terms of the physics-to-physics conversion efficiency and the mechanical interface coupling between the magnetostrictive core and piezoelectric shell in MENPs to determine the degree of magnetoelectricity. Various methods have been investigated to precisely and reliably characterize ME voltage coefficients by reducing the artifact error of small nanoparticles.

Because of the use of a magnetic field, which is harmless to the human body, core–shell MENPs are suitable for medical applications that require the generation of an electric field in a material with low magnetic permeability, such as a human body or an ionic liquid solution [40–42]. Therefore, core–shell MENPs are expanding their range of applications [43] to biomedicine for brain stimulation [44], cell regeneration [45], imaging [46], drug delivery and release [47], as well as electrocatalysts for water purification [48], as illustrated in Figure 1.

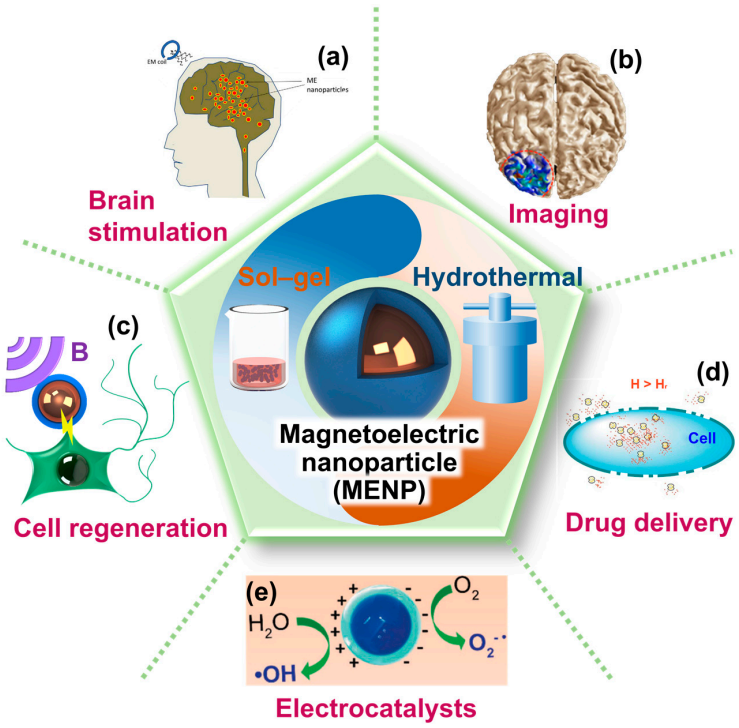

Figure 1. Schematic summary showing the synthesis methods of magnetoelectric nanoparticles (MENPs), such as sol–gel and hydrothermal, and their various biomedical and environmental applications. (**a**) Brain stimulation. Reproduced with permission from [49]. Copyright 2012, PLoS ONE. (**b**) Brain imaging. Reproduced with permission from [50]. Copyright 2018, BMC Springer Nature. (**c**) Cell regeneration. Reproduced with permission from [45]. Copyright 2022, Royal Society of Chemistry. (**d**) Drug delivery that induces nano electroporation. Reproduced with permission from [51]. Copyright 2013, Nature. (**e**) Electrocatalysts for water purification. Reproduced with permission from [48]. Copyright 2019, Wiley-VCH.

For instance, by stimulating the brain with an electric field generated from MENPs caused by an applied magnetic field, several diseases can be treated, and neuronal cell regeneration (differentiation and proliferation) can also be accelerated. Moreover, the electric field generated from MENPs can open channels in the cell membrane and release drugs loaded on the large surface of the MENPs [52]. It is also possible to create an image of the structure of tissues by sensing the magnetic field induced by MENPs owing to electric signals generated from the human body through the converse magnetoelectric effect and mapping their positions. Moreover, for electrocatalysts, a large surface area and electrical asymmetry are required to generate sufficient surface charge to induce an ionic reaction in the solution. Thus, MENPs are promising candidates for electrocatalysis [48].

This review article presents an overview of studies on the materials used and their synthesis strategies, the mechanism of the magnetoelectric phenomenon, ME measurements of various core–shell MENPs, and their biomedical and electrocatalytic applications reported in the last decade.

2. Materials and Magnetoelectric Properties of Core–Shell Structured MENPs

Core–shell structured MENPs are multiphase heterostructured ME composites at the nanoscale, as shown in Figure 2a. In such composites, the ME property is achieved by elastic interfacial coupling between the magnetostrictive and piezoelectric phases under a magnetic field [53]. The typical core in MENPs consists of ferromagnetic materials with a spinel structure (AB_2O_4) showing magnetostrictive properties and a high magnetic moment [36]. The shell is typically composed of ferroelectric materials with a perovskite structure (ABO_3), showing spontaneous electric polarization and piezoelectric properties [54]. For instance, the reported ferromagnetic materials for the magnetostrictive core are Fe_3O_4 [55], $NiFe_2O_4$ [56], and $CoFe_2O_4$, and the perovskite materials for the piezoelectric shell are $PbTiO_3$, $BaTiO_3$ [57], and $BiFeO_3$ [58]. Conversely, if the core and shell of the core–shell MENP are the piezoelectric and the magnetostrictive phases, respectively, then when a magnetic field is applied to the MENP, the transmission of the electric field generated from the piezoelectric core to the surrounding area is partially shielded by the shell, resulting in transmission of electric energy to tissue or reactants in the surroundings of the MENP. The smart combination of appropriate materials is crucial for the large ME effects of MENPs. In addition, interfacial coupling between the core and shell is an important factor in increasing the mechanical transmission from the magnetostrictive core to the piezoelectric shell. For this, well-defined boundaries between different phases without interfacial chemical diffusion due to the low synthesis temperature enhance elastic interfacial coupling, thus resulting in high ME while simultaneously ensuring high chemical, thermal, and mechanical stability.

The underlying mechanism of the ME coupling in MENPs is shown in Figure 2b. In particular, the dielectric asymmetry generated in MENPs results in an electric field, which is spread to the surrounding area under the influence of alternating magnetic fields (Figure 2b(i)). For most applications, an electric potential is induced on the surface of the MENPs from alternating electrical polarization. First, under an alternating magnetic field, vibrational lattice strain in the magnetostrictive core occurs and is transferred to the piezoelectric shell as stress through the mechanical interface coupling between different phases of the core and shell [60,61]. Through the piezoelectric conversion from stress to electric polarization, an electric field is continuously generated in the MENPs with repetitive application and removal of the magnetic field, as shown in Figure 2b(ii). This induces an electric field in the surface of MENPs and additionally induces charge carriers, i.e., electrons (e^-) and holes (h^+) in tissue.

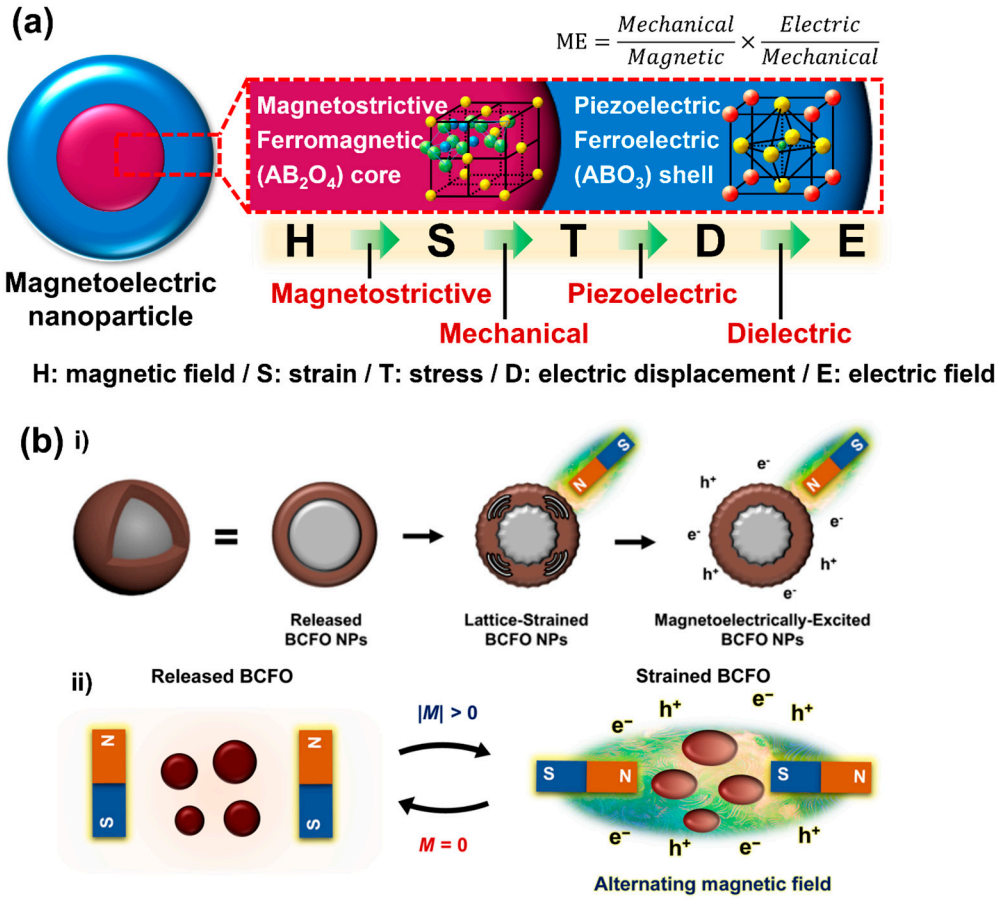

Figure 2. Magnetoelectric (ME) effect of MENPs. (**a**) Concept of physics; transmission mechanism through ME effect in the MENPs composed of the magnetostrictive core and piezoelectric shell. (**b**) (i) The schematic illustration showing that MENPs induce an ME effect when an alternating magnetic field is applied. (ii) Repeatedly induced strain and release of the MENPs dependent on the magnetic moments of the applied magnetic field. Reproduced with permission from [59]. Copyright 2022, Science.

3. Common Synthesis Strategies of Core–Shell Structured MENPs

MENPs can be synthesized by bottom-up methods such as hydrothermal, sol–gel, solvent evaporation, and solid-state reactions. Among these, the sol–gel and hydrothermal syntheses are the most widely used to synthesize magnetostrictive and piezoelectric phases in core–shell structured MENPs. The sol–gel method is appropriate for obtaining the desired particle size because the synthesis conditions can be easily controlled by adjusting the pH, temperature, and concentration [62]. For this, a homogeneous precursor solution, in which the initial material is ionized through hydrolysis, is prepared by dissolving the initial material in a solvent with an appropriate pH and increasing the reaction temperature. After the evaporation of the precursor solution, a dehydrated gel is formed through the polycondensation of alkoxides. Finally, nanocrystalline materials are formed through the calcination of the obtained gel at high temperatures. One of the representative works was reported by Song et al., who used the sol–gel method to synthesize core–shell $CoFe_2O_4$@$BaTiO_3$ (CFO@BTO) MENPs consisting of piezoelectric $BaTiO_3$ shells on magnetostrictive $CoFe_2O_4$ cores, as shown in Figure 3a [45]. To coat the BTO shells on the CFO cores, $BaCO_3$ and $Ti(OCH(CH_3)_2)_4$ were dissolved in a citric acid solution to generate Ba and Ti ions. Next, the CFO nanoparticles were added to the precursor solution containing Ba^{2+} and Ti^{4+}. Gelation around the CFO cores was induced by evaporating the precursor solution. Finally, MENPs with a shell nanoarchitecture of BTO and a size of 50 nm were obtained by thermal annealing.

The hydrothermal method provides the advantages of increased solubility and fast reaction of precursors at elevated temperatures and pressure in an autoclave, thus reducing the energy and cost required for the reaction [63–65]. First, the precursor solution composed of the starting materials forms an amorphous layer containing B-site ions in the perovskite structure (ABO_3) through hydrolysis and aging (Figure 3b). Subsequently, during the hydrothermal reaction using the autoclave, A-site ions are incorporated into the amorphous layer around the supercritical point of water. Rongzheng et al. chose Fe_3O_4@$PbTiO_3$ core–shell particles to demonstrate the effectiveness of the hydrothermal synthesis method [66]. To coat Fe_3O_4 nanoparticles synthesized using the hydrothermal method with $PbTiO_3$ shells, Ti^{4+} ions from the $Ti(SO_4)_2$ precursor formed a smooth layer on the Fe_3O_4 nanoparticles through an aging process. Then, nanocrystalline $PbTiO_3$ shells were formed by integrating A-site Pb^{2+} ions into the Ti hydroxide layer, at relatively low temperatures owing to the high-pressure process in the autoclave. In addition, annealing was performed to obtain more crystalline and denser core–shell Fe_3O_4@$PbTiO_3$ particles.

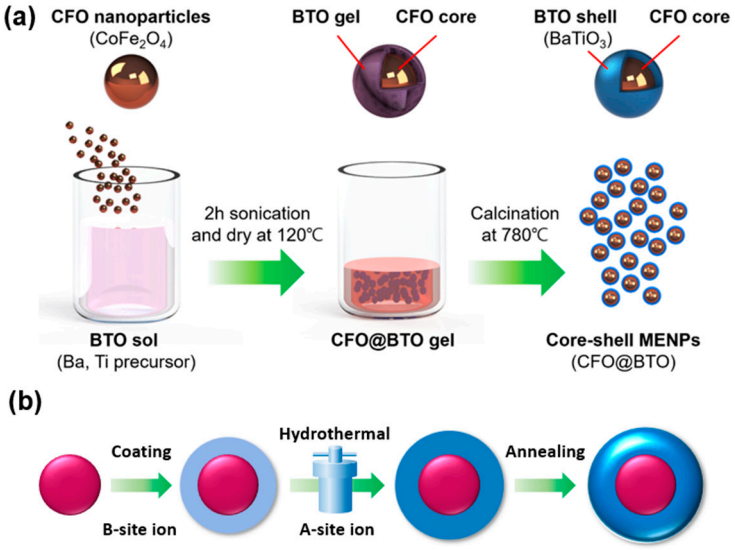

Figure 3. Widely adopted fabrication methods of MENPs with core–shell structure. (**a**) Preparation of $CoFe_2O_4$@$BaTiO_3$ (CFO@BTO) MENPs using the sol–gel method. Reproduced with permission from [45]. Copyright 2022, Royal Society of Chemistry. (**b**) Synthesis of core–shell MENPs employing the hydrothermal method. Reproduced with permission from [67]. Copyright 2010, Royal Society of Chemistry.

Additionally, the solid-state reaction was used to mechanically fabricate MENPs with an irregular structure rather than a clear core–shell structure [67]. For this, the piezoelectric BTO and magnetostrictive $Ni_{0.5}Co_{0.5}Fe_2O_4$ (NCF) were milled and mixed to synthesize BTO–NCF MENPs. The solid-state reaction is based on mechanical mixing and solid-state diffusion of ions at high temperatures. In addition, single-grain BTO-($Mn_{0.5}Zn_{0.5}$)Fe_2O MENPs with varying geometrical shapes were synthesized employing the solid-state reaction [68]. Other synthesis methods, such as microemulsion-based, solvent evaporation, and sonochemical syntheses, have been carried out to fabricate ferroelectric and ferromagnetic nanocrystals. During microemulsion-based synthesis, nanocrystal precipitation occurs due to chemical reactions of inorganic salts and the removal of water. Using this method, MENPs containing CFO [69] and BFO [70] could be successfully synthesized. The solvent evaporation method is suitable for the synthesis of pure MENPs because of the easy removal of impurities from the solution during evaporation. Thus, $BiFeO_3$ was synthesized by drying metal ions mixed with organic molecules after solvent evaporation and calcination [71]. During the sonochemical synthesis, nanoclusters agglomerate due to the implosive collapse of bubbles produced by acoustic cavitation, and perovskite nanocrystals, such as $SrTiO_3$ nanoparticles, can be formed after additional calcination [72].

4. Magnetoelectricity Measurements of Core–Shell Structured MENPs

It is crucial to characterize the ME coupling of MENPs to provide reliable data for specific applications. ME coupling, which is described with the ME voltage coefficient (α_{ME}), is a result of mechanical interfacial coupling between the magnetostrictive core and piezoelectric shell, and can be expressed as [45]:

$$\alpha_{ME} = p \times \lambda = \frac{\Delta E}{\Delta S} \times \frac{\Delta S}{\Delta H} = \frac{\Delta E}{\Delta H} = \frac{\Delta V/t}{\Delta H} \ (Vcm^{-1}Oe^{-1}), \quad (1)$$

where p and λ are piezoelectric and magnetostrictive coefficients, respectively, ΔE is the electric field change induced by the ME effect, ΔS is the strain change generated by the magnetostrictive core, and ΔH is the applied external magnetic field. The electric field is defined as the voltage change (ΔV) divided by the thickness (t) of the piezoelectric shell. Based on this ideal definition of the ME voltage coefficient, the exact values can be obtained by measuring the output voltage signals induced by the MENPs under an applied magnetic field. Generally, ME measurements are conducted under a dynamically changing alternating magnetic field (H_{AC}) superimposed with a direct-current magnetic field bias (H_{DC}) [73,74], and the electrical voltage response from the MENPs under the combined magnetic field is measured using a lock-in amplifier. To obtain a sufficiently large electrical signal relative to the noise, the sum of electrical signals is measured from multiple MENPs of the bulk ME composite mixed into a polymer matrix followed by curing, as shown in Figure 4a. Based on the results obtained from the dynamic ME measurements of multiple MENPs in a bulk specimen, ME voltage coefficients can be relatively easily determined [75]. However, for the determination of the ME voltage coefficients of a bulk specimen composed of a cured conductive polymer and MENPs, the reduced polarization of the piezoelectric shell, owing to charge leakage caused by the conductive polymer, should be considered.

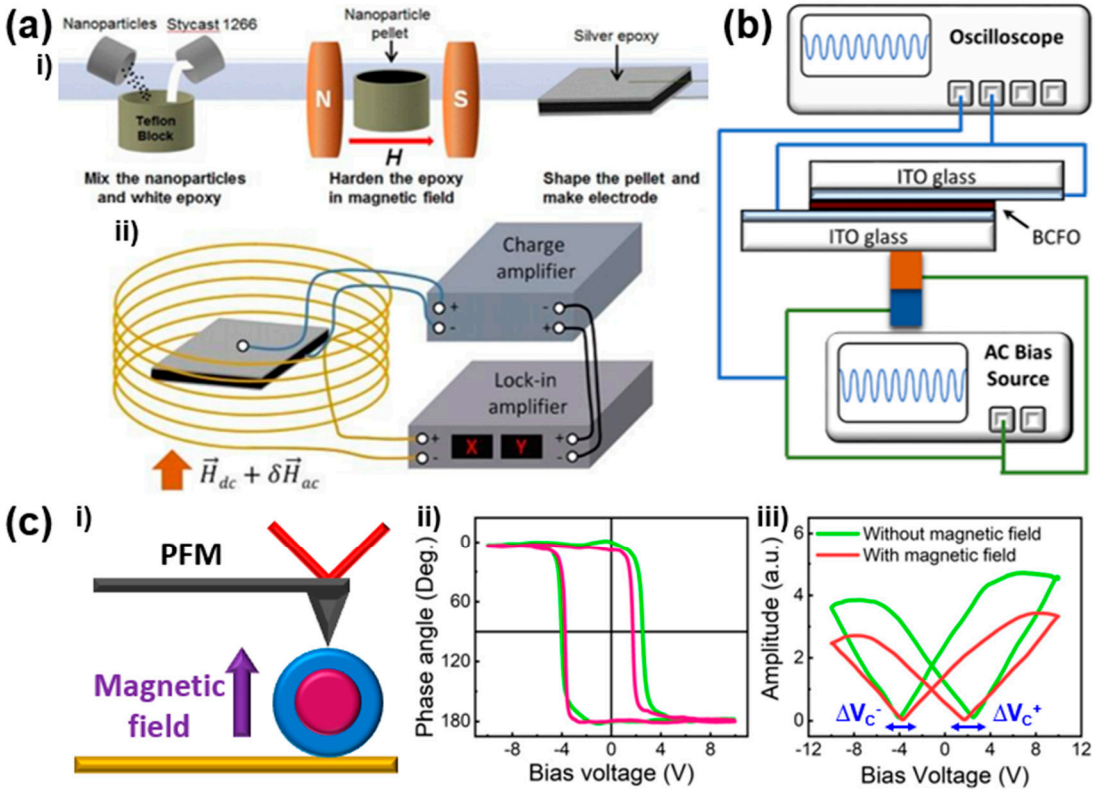

Figure 4. Schematics showing different ME measurement methods of MENPs. (**a**)-(i) Fabrication process of bulk ME composites consisting of MENPs embedded in a polymer matrix, and (ii) dynamic ME measurement setup. Reproduced with permission from [75]. Copyright 2016, American Chemical

Society. (**b**) ME characterization of multiple MENPs placed between two electrodes connected to the oscilloscope under an AC magnetic field. Reproduced with permission from [59]. Copyright 2022, Science. (**c**)-(i) Piezoresponse force microscopy (PFM) probe system for ME measurement of a single MENP, (ii) hysteresis and (iii) bipolar strain vs. electric field (S-E) curves obtained from a single MENP with and without the application of a magnetic field, which is utilized for the calculation of the ME voltage coefficient. Reproduced with permission from [45]. Copyright 2022, Royal Society of Chemistry.

To overcome the limitations of ME measurements for bulk specimens containing MENPs, multiple MENPs were placed between two electrodes, which were connected to an oscilloscope (Figure 4b) [59]. Under a low-frequency alternating magnetic field, MENP-induced response was detected, exhibiting similar waveforms to the applied magnetic field intensity and confirming that the voltage signals resulted from the ME phenomenon activated by the magnetic field. Using this method, amplified voltage signals of MENPs can be obtained with no polarization reduction due to charge leakage and structural change of the material [76]. However, it is insufficient to determine the exact ME voltage coefficient of a single MENP, because it does not consider errors caused by the size deviation of the manufactured MENPs and the generation of large granulated secondary particles by primary particle aggregation.

Precise ME measurements of a single MENP are still challenging because of the small size of the particles. Recently, the modified piezoresponse force microscopy (PFM) probe system for the point I-V method was utilized to directly measure the ME voltage coefficient of a single MENP, as illustrated in Figure 4c(i) [45,59,63]. The ME measurement using a modified PFM probe system is based on the converse piezoelectric effect, which transfers the applied electricity into strain by ME coupling. During the PFM measurement, the directions of the MENP polarization, which switch under the applied electric field, were compared with the piezoresponse hysteresis loops with and without an external magnetic field. The phase angle switching in the hysteresis loops between 0° and 180° with and without a magnetic field indicates that the voltage signals from the MENP measured by PFM can be ascribed to the piezoelectric phenomenon rather than to the electrostatic response (Figure 4c(ii)). The asymmetric shifts of the coercive voltages upon application of an externally applied magnetic field were utilized to calculate the ME voltage coefficient. The difference between the positive ($\Delta V_C{}^+$) and negative ($\Delta V_C{}^-$) coercive voltage shifts with and without a magnetic field in the butterfly loops (S-E curve) represents the charge generated by the polarization of the piezoelectric shell in a single MENP. Thus, the α_{ME} of a single core–shell MENP can be calculated using the following equation [45]:

$$\alpha_{ME} = \frac{\left|\Delta V_C^+ - \Delta V_C^-\right|}{t \times \Delta H} \left(Vcm^{-1}Oe^{-1}\right), \quad (2)$$

where t is the thickness of the piezoelectric shell coated on the magnetostrictive core, and ΔH is the magnetic field applied to a single MENP. ME measurements using the PFM probe system hold a promising opportunity to estimate the α_{ME} of a single MENP, considering its morphology and size without polarization loss. Therefore, ME measurements of a single MENP using probe systems employing PFM [77] or scanning tunneling microscopy (STM) [37] are expected to attract more attention and be actively developed in the future. Table 1 lists various studies related to core–shell MENPs, presenting a comparison of ME voltage coefficient values, syntheses, ME measurement methods, and applications of MENPs. It is worth noting that ME voltage coefficients of single MENPs attained by point I-V ME measurements utilizing point probe systems, such as PFM and STM, show relatively larger values than those obtained from dynamic and oscilloscopic ME measurements of bulk ME composites and multiple MENPs.

Table 1. Comparison of materials, syntheses, ME voltage coefficients, ME measurement method, and applications of MENPs.

Authors (Year)	Material		Synthesis Method	ME Voltage Coefficient (V/cm.·Oe)	ME Measurement Method	Application
	Magnetostrictive Core	Piezoelectric Shell				
Chaudhuri et al. (2015) [78]	$CoFe_2O_4$ (CFO)	$BaTiO_3$ (BTO)	Hydrothermal/Sol–gel method	0.00813	Dynamic ME measurement (Bulk composite)	-
Rao et al. (2017) [79]	$CoFe_2O_4$ (CFO)	$BaTiO_3$ (BTO)	Sol–gel method	0.00918		Drug Delivery
Kozielski et al. (2021) [80]	$CoFe_2O_4$ (CFO)	$BaTiO_3$ (BTO)	Sol–gel method	0.00000276		Brain Stimulation
Almessiere et al. (2022) [81]	$CoMnRFeO_4$ (CoMnRFe)	$BaTiO_3$ (BTO)	Sol–gel method	0.0249		Drug Delivery
Park et al. (2022) [59]	$CoFe_2O_4$ (CFO)	$BiFeO_3$ (BFO)	Sol–gel method	10~30	Oscilloscopic ME measurements (Multiple MENPs)	Brain Stimulation
Pane et al. (2019) [48]	$CoFe_2O_4$ (CFO)	$BiFeO_3$ (BFO)	Hydrothermal/Sol–gel method	405	Point I-V ME measurement (Single MENPs)	Electrocatalysts
Mushtaq et al. (2019) [63]	$CoFe_2O_4$ (CFO)	$BiFeO_3$ (BFO)	Hydrothermal method	1400		Cell Regeneration
Fan et al. (2021) [77]	Fe_3O_4 (FO)	$BaTiO_3$ (BTO)	Hydrothermal/Sol–gel method	260		Brain Stimulation
Song et al. (2022) [45]	$CoFe_2O_4$ (CFO)	$BaTiO_3$ (BTO)	Sol–gel method	47		Cell Regeneration
Pane et al. (2022) [82]	$CoFe_2O_4$ (CFO)	$BiFeO_3$ (BFO)	Hydrothermal/Sol–gel method	325		Electrocatalysts
Nelson et al. (2022) [83]	$CoFe_2O_4$ (CFO)	$BiFeO_3$ (BFO)	Hydrothermal/Sol–gel method	1700		Electrocatalysts

5. Applications of MENPs

5.1. Drug Delivery

Conventional drug delivery techniques are effective for the treatment of most common illnesses; however, they might be insufficient for more complex diseases, such as ovarian cancer [51] and AIDS [84], where viral reservoirs remain untouched by traditional drug therapy methods. Therefore, an assisted and enhanced specific drug delivery system is required [85,86]. In this regard, MENPs can revolutionize drug delivery systems due to their superior and desirable characteristics as nanocarriers. Their ability to intrinsically generate electric fields is beneficial for biomedical applications, as living cells possess inherent electrical properties and utilize them extensively for fundamental recovery functions. Moreover, the most unique and advantageous function of MENPs is that excitation can be controlled wirelessly by applying a low-frequency magnetic field.

MENPs as drug delivery nanocarriers enable high-specificity drug delivery, which is directly aligned with current research trends. Magnetic nanoparticles (MNPs) with similar characteristics, such as nonzero magnetic moments, also enable targeted delivery to specific cells. However, drug adsorption and release are uncontrollable and depend on the

biochemical processes of cells. In contrast, the unique piezoelectric shell of MENPs enables the on-demand release of drugs by utilizing the intrinsic electric field generated through the ME effect. It was shown that the drug efficacy of MENPs was significantly increased compared with MNPs acting as nanocarriers [87,88]. The bond-severing mechanism between the therapeutic agents and MENPs was thoroughly studied, as shown in Figure 5a [51]. It was assumed that there is a symmetric ionic bond before a magnetic field is applied and an electric dipole moment is formed. However, through the application of a magnetic field, the induced electric dipole breaks the symmetry, resulting in a break of the already weak bond, while the bond at the other end of the dipole is strengthened. With the ideal excitation of the AC magnetic field, the dipole moment direction is changed, thus uniformly breaking all bonds and releasing the agent. An efficiently controlled electric field not only facilitates the on-demand release of therapeutic agents but also incites electroporation (Figure 5a(i)). This technique has been proven to have an edge over other physical methods for drug delivery, showing much higher drug efficacy because of the direct drug delivery into cells. In this method, an electric field is applied to increase the permeability of the cell membrane or open its pores, thereby increasing the uptake of therapeutic agents. The primary causes of pore opening are: the electrostatic repulsion that dislocates the phospholipid bilayer, and the constant change in the membrane's conductivity. Despite its advantages, the effectiveness of electroporation is strongly dependent on the voltage distribution and duration. Excessively strong and long excitation might lead to undesirable cell death. However, electroporation using MENPs can target specific cells that are in proximity to a low-frequency but specific electric field generated by MENPs; therefore, this is called nano electroporation. Because of the nanoscaled MENPs, the generated electric field is harmless for cells. In addition, nano electroporation significantly increases the uptake of therapeutic agents, improves cell viability, and enables delivery past semipermeable membranes, such as the blood–brain barrier. This study shows a five-fold increase when MENPs were used as carriers, compared with other carriers such as HER-2 antibodies (Figure 5a(ii)).

MENPs also have a great affinity to different types of agents or drugs that require targeted delivery solutions, including antiviral drugs for treating human immunodeficiency virus (HIV), CRISPR-Cas9/gRNA for latent HIV infection, and antiretroviral drug delivery [84,87,90]. The delivery of such drugs was demonstrated by inducing the electroporation, cell targeting, and cell transport of MENPs [89]. Under an AC magnetic field of 50 Oe at 60 Hz, cell permeation, intercellular signaling, and cell electromechanical motion inside human epithelial cells (HEP2) were induced by a single MENP reducing its impedance (Figure 5b(i)). When an AC magnetic field of 40 Oe at 30 Hz, which is low enough not to dislocate the phospholipids on the cell membrane, is applied, MENP can pass through its pathway to the targeted location avoiding reaction with the cells (Figure 5b(ii)). Being continuously exposed to the DC magnetic field of 50 Oe applied through the direction of the outlet of the microchannel, it is proven that MENPs can manipulate the live cells to the targeted area by generating thrust and steering the cells (Figure 5b(iii)). The results of this in vitro study confirmed that the effects of MENPs were largely positive, reporting no significant toxicity. The results of the biocompatibility test on HEP2 and NG-108 rat neuronal cells confirm that MENPs have potential to be used as nanocarriers for enhanced targeted and on-demand release drug delivery with no toxicity.

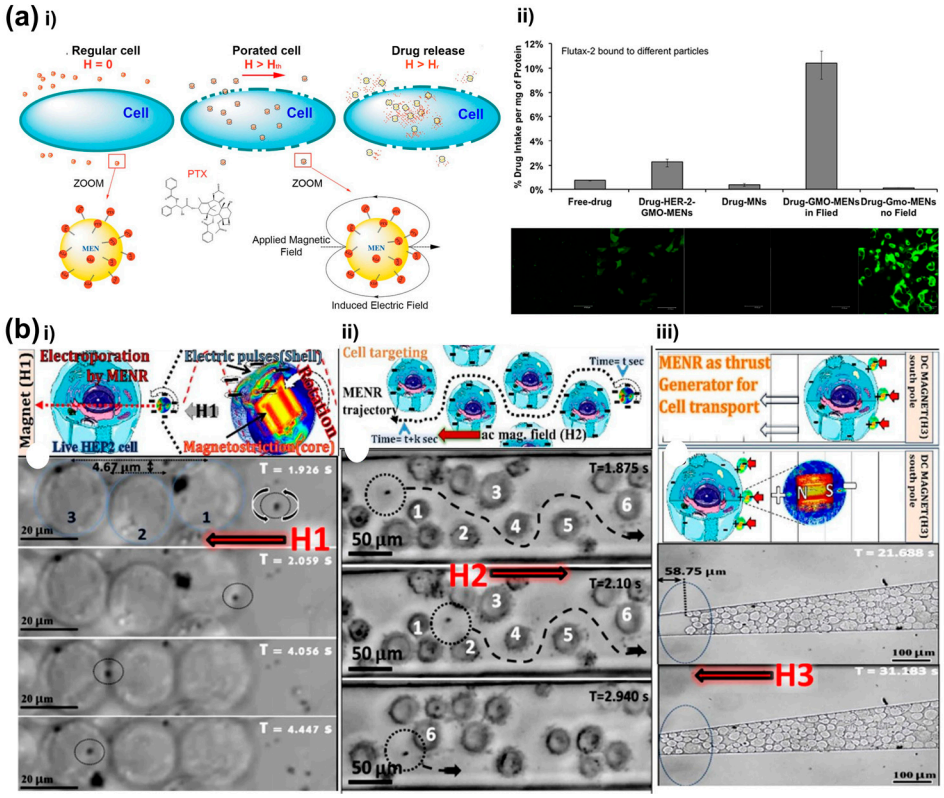

Figure 5. Schematics showing MENP-facilitated drug delivery. (**a**)-(i) Drug uptake via nano electroporation induced by the MENPs, and (ii) verification of the ME effect of MENPs on drug uptake. Reproduced with permission from [51]. Copyright 2013, Nature. (**b**) Penetration of MENPs through or into cells due to the application of a magnetic field, including (i) electroporation, (ii) cell targeting, and (iii) cell transport; the observation is conducted by Betal et al. Reproduced with permission from [89]. Copyright 2018, Nature.

5.2. Brain Imaging

For the noninvasive examination of the brain and other internal organs and tissues, magnetic resonance imaging (MRI) is routinely used to generate high-resolution images and, therefore, MRI equipment has become critical for healthcare in hospitals. MRI enables the noninvasive detection and diagnosis of various diseases, primarily in the brain. In addition, MNPs can be added as a contrast agent to further enhance imaging quality [91]. Currently, magnetic particle imaging (MPI) is an emerging magnetic-based imaging technology [50]. However, there is a fundamental difference between MRI and MPI, as the latter does not detect signals produced from the magnetically aligned atoms; rather, it traces MNPs and detects voltage due to the nonlinear change in magnetization. The voltage is then transformed into a signal, which is transformed into an image. This method is more sensitive because it not only produces a direct image based on the data but can also quantify the change. Theoretically, the image and data are more impactful because they can also map neural activities in more detail. Because MNPs act as tracers rather than contrast agents in MPI, individual particle function correlates with magnetization and might improve the readings. This shows that MENPs with ME effects have potential to further improve the MPI imaging process.

Numerical simulation studies indicate that MENPs can generate small magnetic moments when action potentials travel down neural axons, as can be seen in Figure 6a [50,92]. The exact mechanism is that the magnetic moments of MENPs are flopped near the axons due to their exposure to a reversed local electric field, and can be observed in the local contrast change of the magnetic image. Thus, this method can detect the detailed neural activities of the cells. Furthermore, the change in the action potential of the excitatory post-

synaptic potential generated at the neuron's apical dendritic tree is longer in duration, and theoretically easier to detect, than action potentials. A study demonstrated the possibility of enhancing brain imaging with MENPs using MPI [93]. The advantages of MPI over MRI, such as fast temporal resolution and superior sensitivity, enable the mapping of potential changes, and consequently detailed mapping of brain activity, as shown in Figure 6b. Currently, there are no in vivo studies confirming the enhancement of brain imaging using MENPs; however, computational studies indicate their great potential, and other studies show that MENPs are safe and can be completely secreted in 8 weeks [94]. Further detailed studies on biomedical imaging are required, as they will deepen our understanding of the brain and other body tissues.

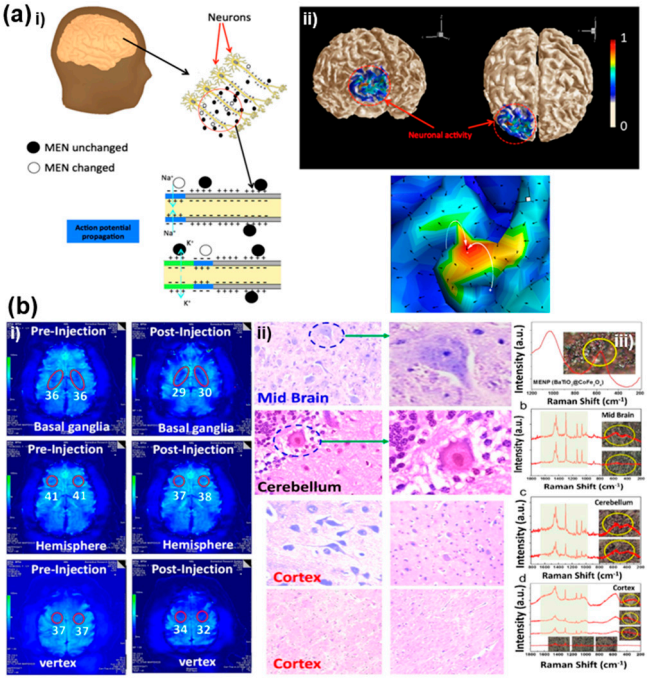

Figure 6. Brain mapping by detecting magnetic signals induced by MENPs located on the targeted brain or other tissues. (**a**)-(i) Magnetic particle imaging (MPI) brain imaging applications enhanced with charge sensing based on the ME phenomenon of the MENPs. (ii) Visualized brain map computationally modeled by placing MENPs on the specific area of the brain. [50]. Copyright 2018, BMC Springer Nature. (**b**)-(i) Scans of magnetic resonance images (MRI) using MENPs delivered to the targeted location of the brain. (ii) Verification of MENP delivery by comparing the morphological assessment of injected MENPs with the scanned position of the MENPs. (iii) Evaluation of MENPs in the organs using Raman spectroscopy. Reproduced with permission from [93]. Copyright 2019, American Chemical Society.

5.3. Brain Stimulation

Brain stimulation using electric fields has proven effective in relieving the symptoms of brain diseases, such as unintended shaking in the case of Parkinson's disease [95]. Conventional brain stimulation therapies, which usually utilize electrodes, are invasive and show unwanted external vibrations. Moreover, the stimulation is not uniform and may have adverse effects owing to energy dissipation. Other less invasive methods, such as transcranial magnetic stimulation (TMS), show a significant disadvantage due to the depth–focal trade-off restricting effective TMS stimulation of the subthalamic region, which is the targeted region in deep brain stimulation (DBS). Other devices that utilize remotely powered concepts using magnetic induction or optoelectronics [96] suffer from shallow penetration depths. The use of MENPs may enable highly uniform brain stimulation and more spatial precision. In addition to its ability to wirelessly incite an electric field, brain

stimulation using the MENP-based technology will be noninvasive, after the initial injection of MENPs, as shown in Figure 7a [49]. Moreover, the spatial distribution of MENPs can be controlled using a magnetic field because of their nonzero magnetic moment. Because the electric field is generated by the ME effect, there is no significant energy dissipation that might damage brain cells. Furthermore, this method may elucidate the mechanisms of neural networks and enhance their imaging. Thus, owing to the unique characteristics of MENPs, they can be considered viable candidates for DBS.

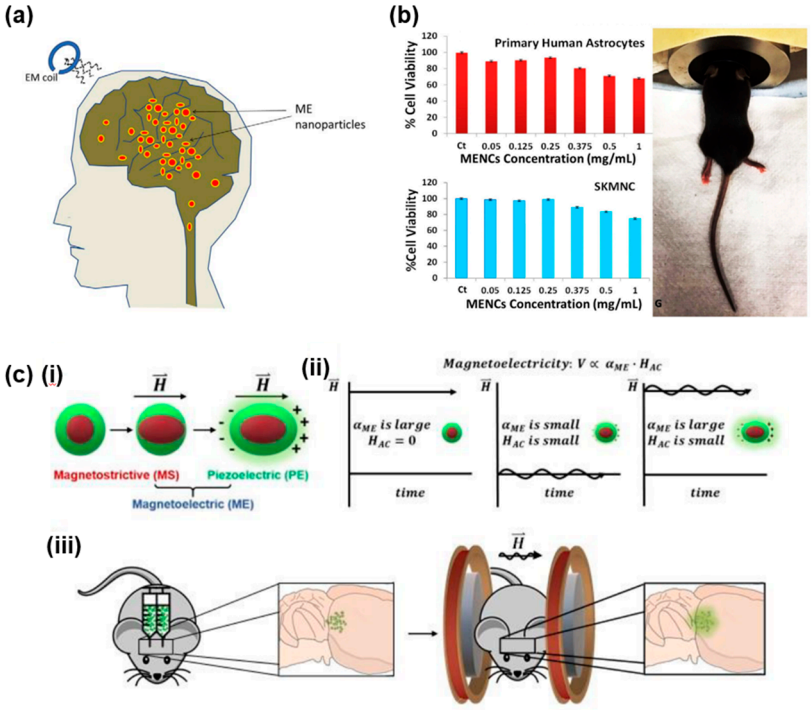

Figure 7. Brain stimulation utilizing the electric field generated from MENPs under the application of the magnetic field. (**a**) Illustration of human brain stimulation using MENPs. Reproduced with permission from [49]. Copyright 2012, PLoS ONE. (**b**) In vivo study on mice showing successful brain stimulation using MENPs. Reproduced with permission from [97]. Copyright 2016, Nature. (**c**)-(i) ME effect generated using MENPs, (ii) external application of combined AC and DC magnetic fields, (iii) in vivo wireless deep brain stimulation. Reproduced with permission from [80]. Copyright 2021, Science.

Although numerous studies have confirmed that the use of MENPs is harmless for living organisms, their effectiveness and safety as brain stimulants require rigorous investigations. A pioneering computational study suggests that the use of MENPs is superior to established methods, such as DBS using implanted electrodes [49]. The study compared typical electric field signals of the brain of a patient with Parkinson's disease exposed to different treatments. The results show that after stimulation using MENPs, the electric field signals of the diseased brain were more similar to those produced by a healthy brain than when subjected to conventional therapies. Following this initial computational study, various effects and phenomena of MENPs for DBS have been observed and thoroughly studied. An in vitro study confirmed an increase in neuronal cell activity by measuring intracellular Ca^{2+} when MENPs were activated with AC and DC magnetic fields [80]. Moreover, the number of c-Fos-positive cells increased significantly in mice; this number is the usual indicator when neurons fire action potentials, as shown in Figure 7b,c [80,97]. The postmortem examination of the mice's brain cells confirmed the increased c-Fos-positive cell number in the nonmotor thalamic region and the absence of neuroinflammation [85]. Owing to their numerous advantages and superior characteristics, MENPs can be considered an

alternative to conventional brain stimulation methods, as they enable the stimulation of the inaccessible subthalamic region.

5.4. Cell Regeneration

In addition to brain-related applications, MENPs are potentially useful for other medical applications as well. MENPs can stimulate cell differentiation, which is an important process in cell regeneration. As shown in Figure 8a, an in vitro study confirmed the ability of MENPs to induce selective differentiation of SH-SY5Y cells using a stamping magnetoelectric microscale biorobot [45]. It is also well known that electric stimulation not only induces differentiation, but is also linked to the proliferation and secretion of proteins, among other effects [98]. While existing electric stimulation methods rely on electrodes and are invasive [99], electrostimulation using MENPs would be noninvasive and could improve stimulation distribution and efficiency. Although piezoelectric materials can also be utilized for noninvasive electrical stimulation in some cases, where an electrical field can be generated through simple exercise or movement, movement is strictly restricted and may damage cells. The simple solution to this issue also lies in the use of MENPs, owing to their unique and convenient characteristics for inducing wireless electric stimulation. This was confirmed by an in vivo study of a patient with a spinal cord injury using a combination of MENPs and biocompatible polymeric materials, which successfully stimulated and fostered the regeneration of functional axons (Figure 8b) [77]. Additionally, stimulation of the brain using the ME effect of MENPs can destroy specific Alzheimer's β-amyloid aggregates, which are possibly responsible for gradual cell degradation, and might improve the function of brain cells, as shown in Figure 8c [59].

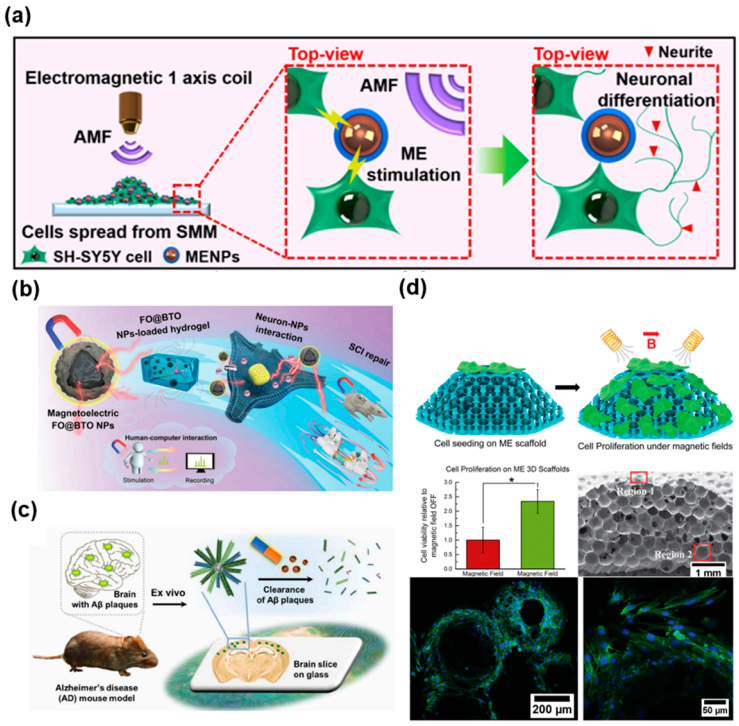

Figure 8. Cell regeneration induced by the ME effect of MENPs. (**a**) Schematic showing enhanced cell differentiation of SH-SY5Y cells through ME stimulation using MENPs. Reproduced with permission from [45]. Copyright 2022, Royal Society of Chemistry. (**b**) Repair of a spinal cord injury due to cell proliferation enhanced by ME stimulation of MENPs. Reproduced with permission from [77]. Copyright 2021, Wiley-VCH. (**c**) Clearance of Aβ plaques, the main indicator of Alzheimer's disease, due to the ME stimulation of MENPs. Reproduced with the permission of [59]. Copyright 2022, Science. (**d**) Bone cell proliferation on ME bioscaffolds containing MENPs under a magnetic field. Reproduced with permission from (*$p < 0.03$) [63]. Copyright 2019, Elsevier.

MENPs can also be coupled with a biocompatible scaffold for bone cell proliferation (Figure 8d) [63]. Scaffolds have been extensively used for this purpose as they efficiently improve the diffusion of oxygen, nutrients, and waste products, which are critical in the early stages before vasculogenesis or angiogenesis. Current bone regeneration research aims for scaffolds that can be compounded with certain biochemical molecules to enable the development of new tissue [100]. Owing to the positive effect of MENPs on cell regeneration, they can be incorporated into scaffolds to enhance the cell proliferation process. Thus, a significant increase in cell proliferation of 134% was achieved using scaffolds combined with magnetically stimulated MENPs. Additional observations of fluorescent images showed that MG63 cells adhered well to the scaffold, indicating successful bone cell proliferation and signifying the importance of MENP-induced electrical stimulation for increased cell viability.

5.5. Electrocatalysts

Proper water treatment is crucial to ensure and maintain the supply of potable water in the future as industrialization expands. MENPs, with their unique characteristics of inciting intrinsic electric fields, have found another field of application aside from biomedicine, namely as catalysts for the degradation of organics in wastewater. Current technology mainly focuses on the use of photocatalysts [101] and magnetic nanostructures [48] as recoverable carriers for catalytic materials to purify water from various common industrial pollutants; however, it does not consider the use of nanoparticles with magnetoelectric properties. It was reported that MENPs can initiate a redox reaction to form hydroxyl and superoxide radicals, resulting in a significantly increased degradation efficiency of organic water pollutants by up to 97% after less than an hour, as shown in Figure 9a [48]. In contrast, other nanoparticles, such as magnetic nanoparticles, did not show the same efficiency within the same period. It was further demonstrated that other common pharmaceuticals could also be removed from water with an efficiency of up to 85% (Figure 9b). This highly efficient performance bodes well for use of MENPs as catalysts in wastewater purification. Despite promising results, the number of related studies is still sparse. However, this approach will certainly be important in the future, given the increasing levels of pollution and current climate changes.

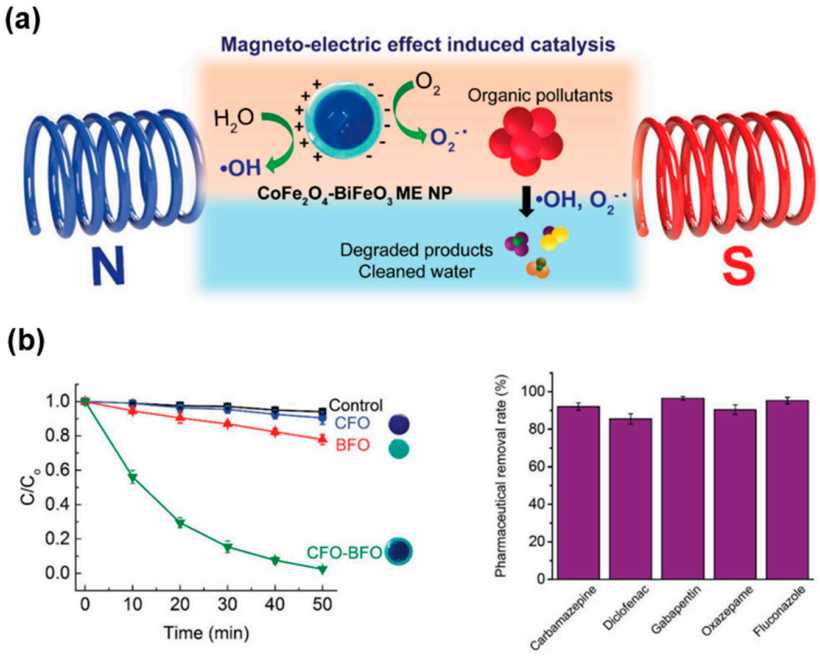

Figure 9. Applications of MENPs as degradation catalysts for wastewater purification. (**a**) Schematic shows the degradation of organic pollutants using MENPs as ME effect-induced catalysts. (**b**)

Effective reduction of the pollutant concentration within 50 min and removal of various common industrial-grade pollutants using MENPS. The figure and data are showcased by Mushtaq et al. Reproduced with permission from [48]. Copyright 2019, Wiley-VCH.

6. Outlook and Perspectives

The ever-increasing variety of applications of nanoparticles is being tremendously boosted by the introduction of nanoparticles with specific functions. Among all these diverse applications, electricity generation in MENPs under magnetic fields shows high potential for application in nonmagnetizable media, putting it in the spotlight in biomedical and environmental fields. In this review, recent progress on core–shell MENPs was introduced, focusing mainly on materials, synthesis methods, ME characteristics, and applications. Core–shell MENPs enjoy high ME voltage coefficients owing to the phase-to-phase elastic interfacial coupling in ME composites, i.e., the high bonding strength of the interface between the magnetostrictive core and piezoelectric shell. Although many characterization methods have been introduced to evaluate the magnetoelectricity of a single MENP, there is still a need to improve these methods to accurately perform ME measurements. These measurements are required to ensure the high quality and efficient performance of MENPs for practical applications where MENPs must be well-dispersed and their characteristics must be uniform. This can be achieved if we minimize the errors resulting from materials, processes, and measurement setups. Dynamic ME measurements with bulk specimens take into account errors caused by charge leakage and thermal deformation during sample preparation. Therefore, any evaluation of multiple MENPs should always be presented with the size deviation errors.

Despite the great advances in MENPs in the last decade, there are still some challenges that need to be addressed to realize the full potential of MENPs in different applications. (i) The asymmetric lattice structure of materials constituting the piezoelectric shell of MENPs, such as BTO, determines its piezoelectric properties. Any reduction in the size of the piezoelectric phase down to the nanoscale is accompanied by a decrease in the ratio of the asymmetric lattice phase, consequently leading to a significant decrease in piezoelectric properties and increasing the dependency of the ME phenomenon on the dielectric properties. Therefore, to attain a large ME effect, it is necessary to improve the material design of MENPs. (ii) Aggregation of nanoparticles should be avoided during the synthesis of MENPs, as it can drastically impact the reproducibility of ME measurements due to nonuniform size distribution and unclear core–shell structures. (iii) Efforts should be directed towards research initiatives to introduce highly scalable synthesis methods for the reproducible and highly efficient mass production of MENPs, mitigating the drawbacks of sol–gel and hydrothermal methods, which are not industrially scalable. (iv) ME measurement techniques should be refined to allow accurate quantification of the ME effect for single MENPs. (v) Finally, as applications of MENPs are increasingly focused on biomedical fields, long-term in vitro and in vivo research is required to improve the understanding of MENPs' working mechanisms. One important task, however, is to avoid cytotoxicity-related issues by either avoiding or reducing the use of toxic solvents and completely removing impurities during the synthesis of MENPs. We therefore propose that these research directions, if implemented, can have huge impacts on the many applications of this emerging field, especially in drug delivery, brain imaging, brain stimulation, cell regeneration, and electrocatalysts.

Author Contributions: Conceptualization, H.S., M.A.L. and J.R.; Writing—original draft preparation, H.S. and M.A.L.; methodology, H.S.; formal analysis, H.S.; investigation, H.S. and M.A.L.; data curation, H.S.; writing—review and editing, H.S. and J.R.; visualization, H.S.; supervision, J.R.; project administration, H.S. and J.R.; funding acquisition, J.R. All authors have read and agreed to the published version of the manuscript.

Funding: This study was supported by the National Research Foundation of Korea (NRF–2022R1F1A1073594).

Data Availability Statement: Not applicable.

Conflicts of Interest: The authors declare no conflict of interest. The founding sponsors had no role in the design of the study; in the collection, analyses, or interpretation of data; in the writing of the manuscript, and in the decision to publish the results.

References

1. Hou, X.; Zaks, T.; Langer, R.; Dong, Y. Lipid Nanoparticles for MRNA Delivery. *Nat. Rev. Mater.* **2021**, *6*, 1078–1094. [CrossRef] [PubMed]
2. Mitchell, M.J.; Billingsley, M.M.; Haley, R.M.; Wechsler, M.E.; Peppas, N.A.; Langer, R. Engineering Precision Nanoparticles for Drug Delivery. *Nat. Rev. Drug Discov.* **2021**, *20*, 101–124. [CrossRef] [PubMed]
3. Astruc, D. Introduction: Nanoparticles in Catalysis. *Chem. Rev.* **2020**, *120*, 461–463. [CrossRef] [PubMed]
4. Wu, H.; Xue, P.; Lu, Y.; Zhu, X. Microstructural, Optical and Magnetic Characterizations of $BiFeO_3$ Multiferroic Nanoparticles Synthesized via a Sol-Gel Process. *J. Alloy. Compd.* **2018**, *731*, 471–477. [CrossRef]
5. Ahmed, M.A.; Mansour, S.F.; El-Dek, S.I.; Abu-Abdeen, M. Conduction and Magnetization Improvement of $BiFeO_3$ Multiferroic Nanoparticles by Ag^+ Doping. *Mater. Res. Bull.* **2014**, *49*, 352–359. [CrossRef]
6. Viehland, D.; Li, J.F.; Yang, Y.; Costanzo, T.; Yourdkhani, A.; Caruntu, G.; Zhou, P.; Zhang, T.; Li, T.; Gupta, A.; et al. Tutorial: Product Properties in Multiferroic Nanocomposites. *J. Appl. Phys.* **2018**, *124*, 061101. [CrossRef]
7. Kirkwood, N.; Singh, B.; Mulvaney, P. Enhancing Quantum Dot LED Efficiency by Tuning Electron Mobility in the ZnO Electron Transport Layer. *Adv. Mater. Interfaces* **2016**, *3*, 1600868. [CrossRef]
8. Zaiats, G.; Ikeda, S.; Kinge, S.; Kamat, P.V. Quantum Dot Light-Emitting Devices: Beyond Alignment of Energy Levels. *ACS Appl. Mater. Interfaces* **2017**, *9*, 30741–30745. [CrossRef]
9. Yang, X.; Mutlugun, E.; Zhao, Y.; Gao, Y.; Leck, K.S.; Ma, Y.; Ke, L.; Tan, S.T.; Demir, H.V.; Sun, X.W. Solution Processed Tungsten Oxide Interfacial Layer for Efficient Hole-Injection in Quantum Dot Light-Emitting Diodes. *Small* **2014**, *10*, 247–252. [CrossRef]
10. Chen, X.Z.; Liu, J.H.; Dong, M.; Müller, L.; Chatzipirpiridis, G.; Hu, C.; Terzopoulou, A.; Torlakcik, H.; Wang, X.; Mushtaq, F.; et al. Magnetically Driven Piezoelectric Soft Microswimmers for Neuron-like Cell Delivery and Neuronal Differentiation. *Mater. Horiz.* **2019**, *6*, 1512–1516. [CrossRef]
11. Liu, L.; Chen, B.; Liu, K.; Gao, J.; Ye, Y.; Wang, Z.; Qin, N.; Wilson, D.A.; Tu, Y.; Peng, F. Wireless Manipulation of Magnetic/Piezoelectric Micromotors for Precise Neural Stem-Like Cell Stimulation. *Adv. Funct. Mater.* **2020**, *30*, 1910108. [CrossRef]
12. Marino, A.; Arai, S.; Hou, Y.; Sinibaldi, E.; Pellegrino, M.; Chang, Y. Piezoelectric Nanoparticle-Assisted Wireless Neuronal Stimulation. *ACS Nano* **2015**, *9*, 7678–7689. [CrossRef]
13. Lee, J.H.; Kim, B.; Kim, Y.; Kim, S.K. Ultra-High Rate of Temperature Increment from Superparamagnetic Nanoparticles for Highly Efficient Hyperthermia. *Sci. Rep.* **2021**, *11*, 4969. [CrossRef]
14. Noh, B.I.; Yang, S.C. Ferromagnetic, Ferroelectric, and Magnetoelectric Properties in Individual Nanotube-Based Magnetoelectric Films of $CoFe_2O_4/BaTiO_3$ Using Electrically Resistive Core-Shell Magnetostrictive Nanoparticles. *J. Alloy. Compd.* **2022**, *891*, 161861. [CrossRef]
15. Gich, M.; Frontera, C.; Roig, A.; Fontcuberta, J.; Molins, E.; Bellido, N.; Simon, C.; Fleta, C. Magnetoelectric Coupling in ε-Fe_2O_3 Nanoparticles. *Nanotechnology* **2006**, *17*, 687–691. [CrossRef]
16. Lotey, G.S.; Verma, N.K. Magnetoelectric Coupling in Multiferroic Tb-Doped BiFeO3 Nanoparticles. *Mater. Lett.* **2013**, *111*, 55–58. [CrossRef]
17. Rajaram Patil, D.; Chai, Y.; Kambale, R.C.; Jeon, B.G.; Yoo, K.; Ryu, J.; Yoon, W.H.; Park, D.S.; Jeong, D.Y.; Lee, S.G.; et al. Enhancement of Resonant and Non-Resonant Magnetoelectric Coupling in Multiferroic Laminates with Anisotropic Piezoelectric Properties. *Appl. Phys. Lett.* **2013**, *102*, 062909. [CrossRef]
18. Ryu, J.; Priya, S.; Uchino, K.; Kim, H.-E. Magnetoelectric Effect in Composites of Magnetostrictive and Piezoelectric Materials. *J. Electroceramics* **2002**, *8*, 107–119. [CrossRef]
19. Ortega, N.; Kumar, A.; Scott, J.F.; Ryu, J.; Carazo, A.V.; Uchino, K.; Kim, H.-E. Magnetoelectric Properties in Piezoelectric and Magnetostrictive Laminate Composites. *Jpn. J. Appl. Phys.* **2001**, *40*, 4948–4951. [CrossRef]
20. Nan, C.W.; Bichurin, M.I.; Dong, S.; Viehland, D.; Srinivasan, G. Multiferroic Magnetoelectric Composites: Historical Perspective, Status, and Future Directions. *J. Appl. Phys.* **2008**, *103*, 031101. [CrossRef]
21. Zhai, J.; Xing, Z.; Dong, S.; Li, J.; Viehland, D. Magnetoelectric Laminate Composites: An Overview. *J. Am. Ceram. Soc.* **2008**, *91*, 351–358. [CrossRef]
22. Pradhan, D.K.; Kumari, S.; Rack, P.D. Magnetoelectric Composites: Applications, Coupling Mechanisms, and Future Directions. *Nanomaterials* **2020**, *10*, 2072. [CrossRef] [PubMed]
23. Chu, Z.; Pourhosseiniasl, M.; Dong, S. Review of Multi-Layered Magnetoelectric Composite Materials and Devices Applications. *J. Phys. D Appl. Phys.* **2018**, *51*, 243001. [CrossRef]
24. Liang, X.; Dong, C.; Chen, H.; Wang, J.; Wei, Y.; Zaeimbashi, M.; He, Y.; Matyushov, A.; Sun, C.; Sun, N. A Review of Thin-Film Magnetoelastic Materials for Magnetoelectric Applications. *Sensors* **2020**, *20*, 1532. [CrossRef] [PubMed]
25. Palneedi, H.; Annapureddy, V.; Priya, S.; Ryu, J. Status and Perspectives of Multiferroic Magnetoelectric Composite Materials and Applications. *Actuators* **2016**, *5*, 9. [CrossRef]

26. Wang, Y.; Gray, D.; Berry, D.; Gao, J.; Li, M.; Li, J.; Viehland, D. An Extremely Low Equivalent Magnetic Noise Magnetoelectric Sensor. *Adv. Mater.* **2011**, *23*, 4111–4114. [CrossRef]
27. Zhai, J.; Xing, Z.; Dong, S.; Li, J.; Viehland, D. Detection of Pico-Tesla Magnetic Fields Using Magneto-Electric Sensors at Room Temperature. *Appl. Phys. Lett.* **2006**, *88*, 062510. [CrossRef]
28. Shah, S. Multiferroics: Towards a Magnetoelectric Memory Related Papers. *Nat. Mater.* **2008**, *7*, 425–426.
29. Israel, C.; Kar-Narayan, S.; Mathur, N.D. Converse Magnetoelectric Coupling in Multilayer Capacitors. *Appl. Phys. Lett.* **2008**, *93*, 173501. [CrossRef]
30. Kambale, R.C.; Yoon, W.H.; Park, D.S.; Choi, J.J.; Ahn, C.W.; Kim, J.W.; Hahn, B.D.; Jeong, D.Y.; Chul Lee, B.; Chung, G.S.; et al. Magnetoelectric Properties and Magnetomechanical Energy Harvesting from Stray Vibration and Electromagnetic Wave by Pb(Mg1/3Nb 2/3)O_3-Pb(Zr,Ti)O_3 Single Crystal/Ni Cantilever. *J. Appl. Phys.* **2013**, *113*, 204108. [CrossRef]
31. Zhuang, X.; Leung, C.M.; Sreenivasulu, G.; Gao, M.; Zhang, J.; Srinivasan, G.; Li, J.; Viehland, D. Upper Limit for Power Conversion in Magnetoelectric Gyrators. *Appl. Phys. Lett.* **2017**, *111*, 163902. [CrossRef]
32. Li, N.; Liu, M.; Zhou, Z.; Sun, N.X.; Murthy, D.V.B.; Srinivasan, G.; Klein, T.M.; Petrov, V.M.; Gupta, A. Electrostatic Tuning of Ferromagnetic Resonance and Magnetoelectric Interactions in Ferrite-Piezoelectric Heterostructures Grown by Chemical Vapor Deposition. *Appl. Phys. Lett.* **2011**, *99*, 192502. [CrossRef]
33. Yan, Y.; Geng, L.D.; Tan, Y.; Ma, J.; Zhang, L.; Sanghadasa, M.; Ngo, K.; Ghosh, A.W.; Wang, Y.U.; Priya, S. Colossal Tunability in High Frequency Magnetoelectric Voltage Tunable Inductors. *Nat. Commun.* **2018**, *9*, 4998. [CrossRef]
34. Kim, D. Planar Magneto-Dielectric Metasubstrate for Miniaturization of a Microstrip Patch Antenna. *Microw. Opt. Technol. Lett.* **2012**, *54*, 2871–2874. [CrossRef]
35. Song, H.; Hwang, G.-T.; Ryu, J.; Choi, H. Stable Output Performance Generated from a Magneto-Mechano-Electric Generator Having Self-Resonance Tunability with a Movable Proof Mass. *Nano Energy* **2022**, *101*, 107607. [CrossRef]
36. Sebastian, V. Design of Magnetostrictive Nanoparticles for Magnetoelectric Composites. *Mater. Chem. Front.* **2017**, *6*, 1368–1390. [CrossRef]
37. Wang, P.; Zhang, E.; Toledo, D.; Smith, I.T.; Navarrete, B.; Furman, N.; Hernandez, A.F.; Telusma, M.; McDaniel, D.; Liang, P.; et al. Colossal Magnetoelectric Effect in Core-Shell Magnetoelectric Nanoparticles. *Nano Lett.* **2020**, *20*, 5765–5772. [CrossRef]
38. Gao, R.; Xue, Y.Z.; Wang, Z.; Chen, G.; Fu, C.; Deng, X.; Lei, X.; Cai, W. Effect of Particle Size on Magnetodielectric and Magnetoelectric Coupling Effect of $CoFe_2O_4$@$BaTiO_3$ Composite Fluids. *J. Mater. Sci. Mater. Electron.* **2020**, *31*, 9026–9036. [CrossRef]
39. Venkata Siva, K.; Kaviraj, P.; Arockiarajan, A. Improved Room Temperature Magnetoelectric Response in $CoFe_2O_4$-$BaTiO_3$ Core Shell and Bipolar Magnetostrictive Properties in $CoFe_2O_4$. *Mater. Lett.* **2020**, *268*, 127623. [CrossRef]
40. Khizroev, S.; Liang, P. Engineering Future Medicines with Magnetoelectric Nanoparticles: Wirelessly Controlled, Targeted Therapies. *IEEE Nanotechnol. Mag.* **2020**, *14*, 23–29. [CrossRef]
41. Khizroev, S. Technobiology's Enabler: The Magnetoelectric Nanoparticle. *Cold Spring Harb. Perspect. Med.* **2019**, *9*, a034207. [CrossRef] [PubMed]
42. Chen, R.; Canales, A.; Anikeeva, P. Neural Recording and Modulation Technologies. *Nat. Rev. Mater.* **2017**, *2*, 16093. [CrossRef] [PubMed]
43. Hoque Apu, E.; Nafiujjaman, M.; Sandeep, S.; Makela, A.V.; Khaleghi, A.; Vainio, S.; Contag, C.H.; Li, J.; Balasingham, I.; Kim, T.; et al. Biomedical Applications of Multifunctional Magnetoelectric Nanoparticles. *Mater. Chem. Front.* **2022**, *6*, 1368–1390. [CrossRef]
44. Kujawska, M.; Kaushik, A. Exploring Magneto-Electric Nanoparticles (MENPs): A Platform for Implanted Deep Brain Stimulation. *Neural Regen. Res.* **2023**, *18*, 129–130. [CrossRef] [PubMed]
45. Song, H.; Kim, D.; Abbasi, S.A.; Latifi Gharamaleki, N.; Kim, E.; Jin, C.; Kim, S.; Hwang, J.; Kim, J.-Y.; Chen, X.-Z.; et al. Multi-Target Cell Therapy Using a Magnetoelectric Microscale Biorobot for Targeted Delivery and Selective Differentiation of SH-SY5Y Cells via Magnetically Driven Cell Stamping. *Mater. Horiz.* **2022**, *9*, 3031–3038. [CrossRef]
46. Guduru, R. *Bionano Electronics: Magneto-Electric Nanoparticles for Drug Delivery, Brain Stimulation and Imaging Applications*; Florida International University: Miami, FL, USA, 2013.
47. el Azim, H.A. Magneto-Electric Nanocarriers for Drug Delivery: An Overview. *J. Drug Deliv. Sci. Technol.* **2017**, *37*, 46–50. [CrossRef]
48. Mushtaq, F.; Chen, X.; Torlakcik, H.; Steuer, C.; Hoop, M.; Siringil, E.C.; Marti, X.; Limburg, G.; Stipp, P.; Nelson, B.J.; et al. Magnetoelectrically Driven Catalytic Degradation of Organics. *Adv. Mater.* **2019**, *31*, 1901378. [CrossRef]
49. Yue, K.; Guduru, R.; Hong, J.; Liang, P.; Nair, M.; Khizroev, S. Magneto-Electric Nano-Particles for Non-Invasive Brain Stimulation. *PLoS ONE* **2012**, *7*, e44040. [CrossRef]
50. Guduru, R.; Liang, P.; Yousef, M.; Horstmyer, J.; Khizroev, S. Mapping the Brain's Electric Fields with Magnetoelectric Nanoparticles. *Bioelectron. Med.* **2018**, *4*, 10. [CrossRef]
51. Guduru, R.; Liang, P.; Runowicz, C.; Nair, M.; Atluri, V.; Khizroev, S. Magneto-Electric Nanoparticles to Enable Field-Controlled High-Specificity Drug Delivery to Eradicate Ovarian Cancer Cells. *Sci. Rep.* **2013**, *3*, 2953. [CrossRef]
52. Mhambi, S.; Fisher, D.; Tchoula Tchokonte, M.B.; Dube, A. Permeation Challenges of Drugs for Treatment of Neurological Tuberculosis and Hiv and the Application of Magneto-Electric Nanoparticle Drug Delivery Systems. *Pharmaceutics* **2021**, *13*, 1479. [CrossRef]

53. Betal, S.; Dutta, M.; Cotica, L.F.; Bhalla, A.S.; Guo, R. Control of Crystalline Characteristics of Shell in Core-Shell Magnetoelectric Nanoparticles Studied Using HRTEM and Holography. *Ferroelectrics* **2016**, *503*, 68–76. [CrossRef]
54. Reaz, M.; Haque, A.; Ghosh, K. Synthesis, Characterization, and Optimization of Magnetoelectric $BaTiO_3$ –Iron Oxide Core–Shell Nanoparticles. *Nanomaterials* **2020**, *10*, 563. [CrossRef]
55. Tanasă, E.; Andronescu, E.; Cernea, M.; Oprea, O.C. $Fe_3O_4/BaTiO_3$ Composites with Core-Shell Structure. *Bull. Ser. B* **2019**, *81*, 171–180.
56. Ryu, H.; Murugavel, P.; Lee, J.H.; Chae, S.C.; Noh, T.W.; Oh, Y.S.; Kim, H.J.; Kim, K.H.; Jang, J.H.; Kim, M.; et al. Magnetoelectric Effects of Nanoparticulate Pb(Zr0.52Ti 0.48)O_3-$NiFe_2O_4$ Composite Films. *Appl. Phys. Lett.* **2006**, *89*, 102907. [CrossRef]
57. Corral-Flores, V.; Bueno-Baqués, D.; Ziolo, R.F. Synthesis and Characterization of Novel $CoFe_2O_4$-$BaTiO_3$ Multiferroic Core-Shell-Type Nanostructures. *Acta Mater.* **2010**, *58*, 764–769. [CrossRef]
58. Zhu, Q.; Xie, Y.; Zhang, J.; Liu, Y.; Zhan, Q.; Miao, H.; Xie, S. Multiferroic $CoFe_2O_4$-$BiFeO_3$ Core-Shell Nanofibers and Their Nanoscale Magnetoelectric Coupling. *J. Mater. Res.* **2014**, *29*, 657–664. [CrossRef]
59. Jang, J.; Beum Park, C. Magnetoelectric Dissociation of Alzheimer's β-Amyloid Aggregates. *Sci. Adv.* **2022**, *8*, eabn1675. [CrossRef]
60. Pandey, P.; Ghimire, G.; Garcia, J.; Rubfiaro, A.; Wang, X.; Tomitaka, A.; Nair, M.; Kaushik, A.; He, J. Single-Entity Approach to Investigate Surface Charge Enhancement in Magnetoelectric Nanoparticles Induced by AC Magnetic Field Stimulation. *ACS Sens.* **2021**, *6*, 340–347. [CrossRef]
61. Wang, P.; Toledo, D.; Zhang, E.; Telusma, M.; McDaniel, D.; Liang, P.; Khizroev, S. Scanning Probe Microscopy Study of Cobalt Ferrite-Barium Titanate Coreshell Magnetoelectric Nanoparticles. *J. Magn. Magn. Mater.* **2020**, *516*, 167329. [CrossRef]
62. Danks, A.E.; Hall, S.R.; Schnepp, Z. The Evolution of "sol-Gel" Chemistry as a Technique for Materials Synthesis. *Mater. Horiz.* **2016**, *3*, 91–112. [CrossRef]
63. Mushtaq, F.; Torlakcik, H.; Vallmajo-Martin, Q.; Siringil, E.C.; Zhang, J.; Röhrig, C.; Shen, Y.; Yu, Y.; Chen, X.Z.; Müller, R.; et al. Magnetoelectric 3D Scaffolds for Enhanced Bone Cell Proliferation. *Appl. Mater. Today* **2019**, *16*, 290–300. [CrossRef]
64. Hadjikhani, A.; Rodzinski, A.; Wang, P.; Nagesetti, A.; Guduru, R.; Liang, P.; Runowicz, C.; Shahbazmohamadi, S.; Khizroev, S. Biodistribution and Clearance of Magnetoelectric Nanoparticles for Nanomedical Applications Using Energy Dispersive Spectroscopy. *Nanomedicine* **2017**, *12*, 1801–1822. [CrossRef] [PubMed]
65. Stimphil, E.; Nagesetti, A.; Guduru, R.; Stewart, T.; Rodzinski, A.; Liang, P.; Khizroev, S. Physics Considerations in Targeted Anticancer Drug Delivery by Magnetoelectric Nanoparticles. *Appl. Phys. Rev.* **2017**, *4*, 021101. [CrossRef]
66. Liu, R.; Zhao, Y.; Huang, R.; Zhao, Y.; Zhou, H. Multiferroic Ferrite/Perovskite Oxide Core/Shell Nanostructures. *J. Mater. Chem.* **2010**, *20*, 10665–10670. [CrossRef]
67. Lather, S.; Gupta, A.; Dalal, J.; Verma, V.; Tripathi, R.; Ohlan, A. Effect of Mechanical Milling on Structural, Dielectric and Magnetic Properties of $BaTiO_3$–$Ni_{0.5}Co_{0.5}Fe_2O_4$ Multiferroic Nanocomposites. *Ceram. Int.* **2017**, *43*, 3246–3251. [CrossRef]
68. Yang, Y.; Wang, J.; Li, J.-F.; Viehland, D.; Nain, A. Nanoparticles Deposition at Specific Sites Using Aligned Fiber Networks. *Open J. Inorg. Non-Met. Mater.* **2012**, *2*, 55–58. [CrossRef]
69. Rondinone, A.J.; Samia, A.C.S.; Zhang, Z.J. Superparamagnetic Relaxation and Magnetic Anisotropy Energy Distribution in $CoFe_2O_4$ Spinel Ferrite Nanocrystallites. *J. Phys. Chem. B* **1999**, *103*, 6876–6880. [CrossRef]
70. Chhabra, V.; Lal, M.; Maitra, A.N.; Ayyub, P. Nanophase $BaFe_{12}O_{19}$ Synthesized from a Nonaqueous Microemulsion with Ba- and Fe-Containing Surfactants. *J. Mater. Res.* **1995**, *10*, 2689–2692. [CrossRef]
71. Ghosh, S.; Dasgupta, S.; Sen, A.; Maiti, H.S. Low-Temperature Synthesis of Nanosized Bismuth Ferrite by Soft Chemical Route. *J. Am. Ceram. Soc.* **2005**, *88*, 1349–1352. [CrossRef]
72. Dutta, D.P.; Tyagi, A.K. Weak Room Temperature Ferromagnetism and Ferroelectric Behavior in Sonochemically Synthesized Bismuth and Iron Codoped $SrTiO_3$ Nanoparticles. *Mater. Lett.* **2015**, *164*, 368–371. [CrossRef]
73. Betal, S.; Dutta, M.; Cotica, L.F.; Bhalla, A.; Guo, R. $BaTiO_3$ Coated $CoFe_2O_4$-Core-Shell Magnetoelectric Nanoparticles (CSMEN) Characterization. *Integr. Ferroelectr.* **2015**, *166*, 225–231. [CrossRef]
74. Song, H.; Peddigari, M.; Kumar, A.; Lee, S.; Kim, D.; Park, N.; Li, J.; Patil, D.R.; Ryu, J. Enhancement of Magnetoelectric (ME) Coupling by Using Textured Magnetostrictive Alloy in 2-2 Type ME Laminate. *J. Alloy. Compd.* **2020**, *834*, 155124. [CrossRef]
75. Yoo, K.; Jeon, B.G.; Chun, S.H.; Patil, D.R.; Lim, Y.J.; Noh, S.H.; Gil, J.; Cheon, J.; Kim, K.H. Quantitative Measurements of Size-Dependent Magnetoelectric Coupling in Fe_3O_4 Nanoparticles. *Nano Lett.* **2016**, *16*, 7408–7413. [CrossRef]
76. Martins, P.; Silva, M.; Lanceros-Mendez, S. Determination of the Magnetostrictive Response of Nanoparticles via Magnetoelectric Measurements. *Nanoscale* **2015**, *7*, 9457–9461. [CrossRef]
77. Zhang, Y.; Chen, S.; Xiao, Z.; Liu, X.; Wu, C.; Wu, K.; Liu, A.; Wei, D.; Sun, J.; Zhou, L.; et al. Magnetoelectric Nanoparticles Incorporated Biomimetic Matrix for Wireless Electrical Stimulation and Nerve Regeneration. *Adv. Healthc. Mater.* **2021**, *10*, 2100695. [CrossRef]
78. Chaudhuri, A.; Mandal, K. Large Magnetoelectric Properties in $CoFe_2O_4$:$BaTiO_3$ Core-Shell Nanocomposites. *J. Magn. Magn. Mater.* **2015**, *377*, 441–445. [CrossRef]
79. Rao, B.N.; Kaviraj, P.; Vaibavi, S.R.; Kumar, A.; Bajpai, S.K.; Arockiarajan, A. Investigation of Magnetoelectric Properties and Biocompatibility of $CoFe_2O_4$-$BaTiO_3$ Core-Shell Nanoparticles for Biomedical Applications. *J. Appl. Phys.* **2017**, *122*, 164102. [CrossRef]

80. Kozielski, K.L.; Jahanshahi, A.; Gilbert, H.B.; Yu, Y.; Francisco, D.E.; Alosaimi, F.; Temel, Y.; Sitti, M. Nonresonant Powering of Injectable Nanoelectrodes Enables Wireless Deep Brain Stimulation in Freely Moving Mice. *Sci. Adv.* **2021**, *7*, eabc4189. [CrossRef]
81. Alfareed, T.M.; Slimani, Y.; Almessiere, M.A.; Shirsath, S.E.; Hassan, M.; Nawaz, M.; Khan, F.A.; Al-Suhaimi, E.A.; Baykal, A. Structure, Magnetoelectric, and Anticancer Activities of Core-Shell $Co_{0.8}Mn_{0.2}R_{0.02}Fe_{1.98}O_4$@$BaTiO_3$ Nanocomposites (R = Ce, Eu, Tb, Tm, or Gd). *Ceram. Int.* **2022**, *48*, 14640–14651. [CrossRef]
82. Kim, D.; Efe, I.; Torlakcik, H.; Terzopoulou, A.; Veciana, A.; Siringil, E.; Mushtaq, F.; Franco, C.; von Arx, D.; Sevim, S.; et al. Magnetoelectric Effect in Hydrogen Harvesting: Magnetic Field as a Trigger of Catalytic Reactions. *Adv. Mater.* **2022**, *34*, 2270139. [CrossRef]
83. Mushtaq, F.; Chen, X.Z.; Veciana, A.; Hoop, M.; Nelson, B.J.; Pané, S. Magnetoelectric Reduction of Chromium(VI) to Chromium(III). *Appl. Mater. Today* **2022**, *26*, 101339. [CrossRef]
84. Nair, M.; Guduru, R.; Liang, P.; Hong, J.; Sagar, V.; Khizroev, S. Externally Controlled On-Demand Release of Anti-HIV Drug Using Magneto-Electric Nanoparticles as Carriers. *Nat. Commun.* **2013**, *4*, 1707. [CrossRef] [PubMed]
85. Nguyen, T.; Gao, J.; Wang, P.; Nagesetti, A.; Andrews, P.; Masood, S.; Vriesman, Z.; Liang, P.; Khizroev, S.; Jin, X. In Vivo Wireless Brain Stimulation via Non-Invasive and Targeted Delivery of Magnetoelectric Nanoparticles. *Neurotherapeutics* **2021**, *18*, 2091–2106. [CrossRef]
86. Nagesetti, A.; Rodzinski, A.; Stimphil, E.; Khanal, T.S.C.; Wang, P.; Guduru, R.; Liang, P.; Agoulnik, I.; Horstmyer, J.; Khizroev, S. Multiferroic Coreshell Magnetoelectric Nanoparticles as NMR Sensitive Nanoprobes for Cancer Cell Detection. *Sci. Rep.* **2017**, *7*, 1610. [CrossRef]
87. Stewart, T.S.; Nagesetti, A.; Guduru, R.; Liang, P.; Stimphil, E.; Hadjikhani, A.; Salgueiro, L.; Horstmyer, J.; Cai, R.; Schally, A.; et al. Magnetoelectric Nanoparticles for Delivery of Antitumor Peptides into Glioblastoma Cells by Magnetic Fields. *Nanomedicine* **2018**, *13*, 423–438. [CrossRef]
88. Kaushik, A.; Nikkhah-Moshaie, R.; Sinha, R.; Bhardwaj, V.; Atluri, V.; Jayant, R.D.; Yndart, A.; Kateb, B.; Pala, N.; Nair, M. Investigation of Ac-Magnetic Field Stimulated Nanoelectroporation of Magneto-Electric Nano-Drug-Carrier inside CNS Cells. *Sci. Rep.* **2017**, *7*, 45663. [CrossRef]
89. Betal, S.; Saha, A.K.; Ortega, E.; Dutta, M.; Ramasubramanian, A.K.; Bhalla, A.S.; Guo, R. Core-Shell Magnetoelectric Nanorobot—A Remotely Controlled Probe for Targeted Cell Manipulation. *Sci. Rep.* **2018**, *8*, 1755. [CrossRef]
90. Kaushik, A.; Yndart, A.; Atluri, V.; Tiwari, S.; Tomitaka, A.; Gupta, P.; Jayant, R.D.; Alvarez-Carbonell, D.; Khalili, K.; Nair, M. Magnetically Guided Non-Invasive CRISPR-Cas9/GRNA Delivery across Blood-Brain Barrier to Eradicate Latent HIV-1 Infection. *Sci. Rep.* **2019**, *9*, 3928. [CrossRef]
91. Corr, S.A.; Byrne, S.J.; Tekoriute, R.; Meledandri, C.J.; Brougham, D.F.; Lynch, M.; Kerskens, C.; O'Dwyer, L.; Gun'ko, Y.K. Linear Assemblies of Magnetic Nanoparticles as MRI Contrast Agents. *J. Am. Chem. Soc.* **2008**, *130*, 4214–4215. [CrossRef]
92. Bok, I.; Haber, I.; Qu, X.; Hai, A. In Silico Assessment of Electrophysiological Neuronal Recordings Mediated by Magnetoelectric Nanoparticles. *Sci. Rep.* **2022**, *12*, 8386. [CrossRef]
93. Kaushik, A.; Rodriguez, J.; Rothen, D.; Bhardwaj, V.; Jayant, R.D.; Pattany, P.; Fuentes, B.; Chand, H.; Kolishetti, N.; El-Hage, N.; et al. MRI-Guided, Noninvasive Delivery of Magneto-Electric Drug Nanocarriers to the Brain in a Nonhuman Primate. *ACS Appl. Bio Mater.* **2019**, *2*, 4826–4836. [CrossRef]
94. Shahzad, K.; Mushtaq, S.; Rizwan, M.; Khalid, W.; Atif, M.; Din, F.U.; Ahmad, N.; Abbasi, R.; Ali, Z. Field-Controlled Magneto-electric Core-Shell $CoFe_2O_4$@$BaTiO_3$ Nanoparticles as Effective Drug Carriers and Drug Release in Vitro. *Mater. Sci. Eng. C* **2021**, *119*, 111444. [CrossRef]
95. Pardo, M.; Khizroev, S. Where Do We Stand Now Regarding Treatment of Psychiatric and Neurodegenerative Disorders? Considerations in Using Magnetoelectric Nanoparticles as an Innovative Approach. *WIREs Nanomed. Nanobiotechnology* **2022**, *14*, e1718. [CrossRef]
96. Lee, S.; Cortese, A.J.; Gandhi, A.P.; Agger, E.R.; McEuen, P.L.; Molnar, A.C. A 250 Mm × 57 Mm Microscale Opto-Electronically Transduced Electrodes (MOTEs) for Neural Recording. *IEEE Trans. Biomed. Circuits Syst.* **2018**, *12*, 1256–1266. [CrossRef]
97. Kaushik, A.; Jayant, R.D.; Nikkhah-Moshaie, R.; Bhardwaj, V.; Roy, U.; Huang, Z.; Ruiz, A.; Yndart, A.; Atluri, V.; El-Hage, N.; et al. Magnetically Guided Central Nervous System Delivery and Toxicity Evaluation of Magneto-Electric Nanocarriers. *Sci. Rep.* **2016**, *6*, 25309. [CrossRef]
98. Betal, S.; Dutta, M.; Shrestha, B.; Cotica, L.; Tang, L.; Bhalla, A.; Guo, R. Cell Permeation Using Core-Shell Magnetoelectric Nanoparticles. *Integr. Ferroelectr.* **2016**, *174*, 186–194. [CrossRef]
99. Sisken, B.F.; Walker, J.; Orgel, M. Prospects on Clinical Applications of Electrical Stimulation for Nerve Regeneration. *J. Cell. Biochem.* **1993**, *51*, 404–409. [CrossRef]
100. Zhang, Y.S.; Zhu, C.; Xia, Y. Inverse Opal Scaffolds and Their Biomedical Applications. *Adv. Mater.* **2017**, *29*, 1701115. [CrossRef]
101. Singh, P.; Sharma, K.; Hasija, V.; Sharma, V.; Sharma, S.; Raizada, P.; Singh, M.; Saini, A.K.; Hosseini-Bandegharaei, A.; Thakur, V.K. Systematic Review on Applicability of Magnetic Iron Oxides–Integrated Photocatalysts for Degradation of Organic Pollutants in Water. *Mater. Today Chem.* **2019**, *14*, 100186. [CrossRef]